Cerebral Cortex September 2010;20:2080–2091
doi:10.1093/cercor/bhp281
Advance Access publication January 4, 2010

Functional Deficit and Recovery of Developing Sensorimotor Networks following Neonatal Hypoxic–Ischemic Injury in the Rat

Charles Quairiaux[1], Stéphane V. Sizonenko[2], Pierre Mégevand[3], Christoph M. Michel[3] and Jozsef Z. Kiss[1]

[1]Faculty of Medicine, Department of Fundamental Neurosciences, University of Geneva, 1211 Geneva, Switzerland, [2]Division of development and Growth, Department of Child and Adolescent and [3]Functional Brain Mapping Laboratory, Department of Clinical Neuroscience, Geneva University Hospital, 1211 Geneva, Switzerland

Neonatal hypoxia–ischemia (HI) is the most important cause of brain injury in the newborn. Here we studied structural alterations and functional perturbations of developing large-scale sensorimotor cortical networks in a rat model of moderate HI at postnatal day 3 (P3). At the morphological level, HI led to a disorganized barrel pattern in the somatosensory cortex without detectable histological changes in the motor cortex. Functional effects were addressed by means of epicranial mapping of somatosensory-evoked potentials (SEPs) during the postischemic recovery period. At P10, SEPs were immature and evoked activity was almost restricted to the somatosensory and motor cortices of the contralateral hemisphere. Peak and topographic analyses of epicranial potentials revealed that responses were profoundly depressed in both sensory and motor areas of HI-lesioned animals. At the end of the postnatal period at P21, responses involved networks in both hemispheres. SEP amplitude was still depressed in the injured sensory region, but it completely recovered in the motor area. These results suggest a process of large-scale network plasticity in sensorimotor circuits after perinatal ischemic injury. The model provides new perspectives for investigating the temporal and spatial characteristics of the recovery process following HI and eventually developing therapeutic interventions.

Keywords: cortex, developmental plasticity, evoked potential, hypoxia–ischemia

Introduction

Neonatal hypoxia–ischemia (HI) brain injuries involve both primary destructive effects including neuronal death and secondary maturational disturbances that lead to the abnormal subsequent development of cerebral white and gray matter (Inder et al. 1999, 2005; Volpe 2009). Particularly devastating in the premature infant, neonatal HI often leads to permanent cognitive and motor deficits that can be subtle to severe (Ferriero 2004; McQuillen and Ferriero 2005). Although the impact of perinatal ischemic damage on cortical tissues is well documented, little is known about the functional consequences, in particular the physiology of recovering cortical networks. The emerging view is that functional recovery mainly relies on a dynamic reorganization of large-scale networks (Nudo 2007). How, where, and when these changes take place remains, however, poorly defined.

In order to better understand the consequences of neonatal HI for the subsequent morphological and functional cerebral development and to enable the evaluation of therapeutic strategies, a model of moderate unilateral HI was developed in the rat at postnatal day 3 (P3) (Sizonenko et al. 2003), a stage showing similarities in terms of cerebral development with the premature human brain of 24–28 weeks (Clancy et al. 2001; Craig et al. 2003). HI at P3 does not produce an overt necrotic reaction as observed in other HI models at P7 (Towfighi and Mauger 1998; Vannucci RC and Vannucci SJ 2005) or in adult rats (Carmichael 2005) but rather leads to various degree of neuronal degeneration and gliotic reaction within deep layers of the parietal cortex in the ischemic hemisphere, sparing frontal and midline cortical areas and subcortical regions (Sizonenko et al. 2003). As observed in the encephalopathy of the premature infant (Volpe 2009), lesions more severely affect specific regions and are characterized by diffuse loss of white matter, zones of patchy neuronal degeneration, altered myelination, radial glia disruption, microglia activation, and hypertophic astrocytes with formation of gliotic scares (Sizonenko et al. 2003, 2005, 2007). The functional deficit and the recovery process after this ischemic damage remain unknown.

The primary somatosensory (S1) region of the parietal cortex contains layer IV segregated clusters of neurons termed barrels that represent the facial whiskers in a somatotopic manner, both structurally and functionally (Woolsey and Van der Loos 1970; Welker 1971; Simons 1978; Armstrong-James and Fox 1987). This system is a widely used model to investigate the different forms of cortical plasticity, that is, from developmental plasticity (Foeller and Feldman 2004) to experience-dependent plasticity (Fox 2002; Frostig 2006; Mégevand et al. 2009) and lesion-induced plasticity (Jenkins and Merzenich 1987; Schiene et al. 1999; Troncoso et al. 2004). Here, we report that HI lesion at P3 leads to the disruption of the morphological organization of the somatosensory barrel field in the parietal cortex as observed at P21.

We recently presented a minimally invasive epicranial approach for multielectrode recordings of vibrissal somatosensory-evoked potentials (SEPs) allowing spatiotemporal analysis of the electrical potential maps over the entire brain similar to human electroencephalography (EEG) mapping studies (Troncoso et al. 2004; Mégevand et al. 2008, 2009). We took advantage of this technique to develop a clinically relevant functional analysis of cortical deficit and recovery in the P3 neonatal HI model. We focused on 2 postinjury time points: P10 to characterize early functional deficits and P21 to probe for potential functional recovery. Our results reveal discrete spatially distributed changes in evoked potential maps that may underlie functional recovery.

Materials and Methods

A total of 115 Wistar rats were used in this study. Animal handling procedures were approved by the Office Vétérinaire Cantonal (Geneva) in accordance with Swiss Federal Laws.

Moderate Unilateral HI

HI was conducted as previously described (Sizonenko et al. 2003). Briefly, the right carotid artery of 3-day-old Wistar pups (64–80 h; 7.5–10.5 g) was cauterized under isoflurane anesthesia. After 30-min recovery at 37 °C in 85 ± 5% humidity in an infant incubator, pups were then submitted to a 30-min period of 6% O_2 hypoxia in the same thermoneutral conditions. Pups were then returned to the dam until they reached P10 or P21.

Histology

Animals received an intraperitoneal injection of sodium pentobarbital and were transcardially perfused with 4% paraformaldehyde. For tangential sections, the cerebral cortices of each hemisphere were isolated from the subcortical structures, rinsed in phosphate buffer (pH 7.4), cryoprotected in 30% sucrose–0.9% NaCl, and flattened between 2 glass slides during snap freezing. For oblique coronal sections, blocks were cut from both hemispheres with a 50° angle from the midsagittal plane, cryoprotected in sucrose 30–0.9% NaCl, and snap frozen. Forty-micron-thick serial sections were then cut on a cryostat for subsequent staining with cytochrome oxidase (CO), Nissl substance, or glial fibrillary acidic protein (GFAP). For CO staining, free-floating sections were rinsed in 0.1 M phosphate buffer (pH 7.4)–4% sucrose before exposition to CO. The CO solution consisted of 0.075% cytochrome C (Sigma C 2506, St Louis, MO), 0.04% 3,3′-diaminobenzidine (Sigma), and 0.1 M phosphate buffer–4% sucrose. The sections were placed in CO solution for 3 h at 37 °C until the barrel fields were seen in contrast to the background. Sections were then rinsed 3 times in 0.1 M phosphate buffer solution and water and mounted on gelatin-coated slides. For Nissl staining or GFAP immunostaining, coronal sections were directly placed on gelatin-coated slides. Nissl substance was then stained with cresyl violet. For GFAP, sections were fixed 30 min in 4% paraformaldehyde, washed in 0.1 M phosphate-buffered saline (PBS), and nonspecific binding was blocked by incubating the slides in 0.1 M PBS/0.5% bovine serum albumine (Sigma) for 30 min at room temperature. Slides were then incubated with the primary antibody for GFAP 1:400 (G-A-5, Boehringer-Manheim, Manheim, Germany) in PBS/0.3% Triton overnight at 4 °C and then 60 min at room temperature with secondary goat Alexa 555 anti-rabbit 1/200 (Molecular Probes) in PBS.

Electrophysiological Recordings

Recordings were carried out under isoflurane anesthesia as previously described (Mégevand et al. 2008). Rats were mounted in a stereotaxic frame providing a continuous flow of isoflurane in 20% O_2/80% air. Body temperature was maintained at 37 °C by a rectal thermistor-controlled heating pad (Harvard Homeothermic Blanket System, UK). A subcutaneous dose of bipuvacaine was injected above the skull before the skin was incised and retracted laterally from above the frontal to the occipital bones. Epicranial SEPs were recorded with a custom-made amplifier from an array of 16 stainless steel electrodes 500 μm in diameter placed to cover the entire skull surface without touching head muscles (gain 5000×; band-pass filters 1–500 Hz; final impedance ≈ 50 kOhms). Electrode coordinates from bregma for the right and left hemispheres were (rostrocaudal/mediolateral, see Fig. 3*A*) as follows: at P10, −6/4 mm (e1, e15), −3.5/5 (e2, e14), −3/2.25 (e3, e13), −1/5 (e4, e12), −0.25/2.25 (e5, e11), 1.25/4 (e6, e10), 3.25/2.25 (e7, e9), 1/0 (e8), −5/0 (reference), and ground electrode at 5.5/0; at P21, −7.5/4 mm (e1, e15), −4.75/5 (e2, e14), −3.5/2.25 (e3, e13), −1.5/5 (e4, e12), −0.75/2.25 (e5, e11), 1.25/4 (e6, e10), 3.25/2.25 (e7, e9), 0/0 (e8), −6.25/0 (reference), and ground electrode at 6/0. For intracortical local field potential (LFP) recordings, a craniotomy was performed in the parietal bone and a linear 16-electrode iridium-based probe with 100-μm interelectrode spacing (NeuroNexus Technologies, Ann Arbor, MI) was inserted into the cortex perpendicular to its surface (gain 5000×, band-pass filters 1–500 Hz); the reference electrode was attached to the skin. All differential voltages were digitally converted at 2 KHz (A/D converter DT3004, Data Translation, Marlboro, MA) under the control of custom-made scripts in VEE Pro 6 (Agilent).

Unilateral stimuli were delivered simultaneously to all large whiskers on one side of the snout through a solenoid-based stimulator device (Troncoso et al. 2000) controlled by the acquisition software. Large whiskers on one side of the snout were glued together and inserted in a thin tube attached to the stimulator probe that was then placed 1 cm away from the whisker pad. Each stimulus consisted of 500-μm back-and-forth deflections with 1-ms rise time. Right-sided and left-sided series of 50 stimuli were applied with an interstimulus interval of 9 s.

Data Analyses

Individual SEPs and LFPs were calculated offline by averaging responses 100 ms prestimulus to 500 ms poststimulus. Grand averages were obtained by averaging individual SEP/LFP by groups. All analyses were performed using the Cartool software by Denis Brunet (http://brainmapping.unige.ch/Cartool.htm) and MATLAB (The Mathworks, Natick, MA).

Peak Analyses

Maximum positive (Pos *P*) and negative (Neg *P*) voltage peaks were calculated for each SEP at selected electrodes. Right/left SEP ratios were calculated using the peak-to-peak amplitudes (Pos *P*–Neg *P*). As voltage peak and ratio distributions turned out to be normal, within group and between group comparisons were performed using unpaired or paired 2-tailed *t*-tests, with Bonferroni correction for test repetitions. All values are mean ± standard error of the mean.

Topographic Analyses of Epicranial Potentials

The multichannel evoked potential data were analyzed using methods used in human evoked potential research (Michel et al. 2004). In order to describe the propagation of evoked activity across the brain surface, periods of stable map topographies optimally summarizing the data were determined using *K* means clustering analysis of grand average SEPs as described previously (Mégevand et al. 2008). Potential values were averaged during those periods at each electrode and interpolated with Delaunay triangulations for graphical representations of mean SEP maps. To investigate differences between experimental conditions, we used unpaired pointwise *t*-tests comparing evoked voltage values at each electrode and at each time frame between groups (Vannucci RC and Vannucci SJ 2005). In addition to this exploratory analysis, we performed global spatial analysis of the map topographies using nonparametric randomization procedures as described previously (Mégevand et al. 2009). Briefly, the spatial dissimilarity between maps from different groups was quantified at each time point. The null hypothesis states that there is no topographic difference between maps from both groups. Maps of individual rats from both groups were therefore normalized to the global voltage amplitudes and randomly reallocated to either condition, simulating the situation where the null hypothesis is true, and the spatial dissimilarity was again calculated. A virtual distribution of spatial dissimilarity under the null hypothesis was then obtained by repeating this procedure a large number of times and compared with the spatial dissimilarity of the actual experiment. Periods of different topographies were declared significant when P remained <0.05 for at least 10 consecutive time frames (5 ms).

LFP and Current Source Density Analyses

Two recordings were necessary to span the entire cortical thickness with our multielectrode probe: in the first recording, the uppermost electrode was placed at the level of the cortical surface; in the second recording, the probe was lowered 500 μm deeper, the lowermost electrode reaching 2000-μm depth. Superficial and deep LFPs were then combined using a linearly weighted average for the depths where 2 recordings had been obtained (Mégevand et al. 2008). The 1-dimensional current source density (CSD) yields the spatiotemporal profiles of extracellular current sinks and sources (Mitzdorf 1985; Leung 1990). The CSD was calculated as the second spatial derivative of the LFP along the depth, with the assumption that currents in the x and y directions were negligible and that intracortical conductivity was constant using the following formula: $\mathrm{CSD} = -[V(z + \Delta z, t) - 2V(z, t) + V(z - \Delta z, t)]/\Delta z^2$; where $V(z, t)$ = measured voltage at a subpial depth z, t = time, Δz = 50 μm (Mitzdorf 1985).

Results

Barrel Field Pattern in the Hypoxic–Ischemic Cortex

After neonatal HI, various degrees of astrogliosis can be observed at P21 in layers IV, V, and VI in the parietal cortex

of the right injured hemisphere, including the barrel field region (Fig. 1). Tangential and coronal oblique sections from the right and left hemispheres of 23 HI rats were stained for CO at P21; 17 brains were used for preparing tangential and 6 for coronal oblique sections (Fig. 2). The stereotypical pattern of CO-stained barrels could be clearly identified in all the left hemispheres while it was disrupted in the majority of cases in the right hemispheres. In tangential sections, 12/16 (75%) rat brains showed clear alterations in the right barrel fields' organization. Of these, 5 were severely affected (42%), with highly irregular barrels, numerous fusions of barrels, and thickened interbarrels' space, rendering difficult to distinguish the typical 5-row pattern organization (Fig. 2*A*,*B*). In the 7 remaining cases, barrel fields were only mildly affected (58%), with a small degree of barrel shape irregularities or barrel fusions (Fig. 2*C*,*D*). Coronal sections also revealed clearly abnormal barrel structures in 3/6 of the right hemispheres (Fig. 2*G*,*H*). Tangential sections stained for Nissl substances suggest concomitant alterations of the cytoarchitectonic organization of barrels (Fig. 2*E*,*F*).

Altered SEPs in the Somatosensory Cortex

The SEP recording experimental design is illustrated in Figure 3*A*,*B*. In the lisencephalic rodent brain, the maximal absolute amplitudes of epicranial potentials should be recorded directly over the active cortical area (Mitzdorf 1985; Mégevand et al. 2008). The contralateral S1 is the first cortical region to receive whisker-evoked activity through thalamocortical (TC) fibers of the ventro-basal nucleus (Welker 1971; Killackey 1973; Armstrong-James and Fox 1987). Accordingly, in the P21 rat (Fig. 3*B*), evoked potentials were fastest and strongest at one of the most lateral electrodes corresponding to the position of the contralateral S1 cortex. In almost all animals, using electrode grids specifically designed for P10 or P21 ages, electrodes 12 (right stimulation) and 4 (left stimulation) recorded the largest evoked potentials. The positioning of these electrodes relatively to barrels was checked histologically during preliminary experiments by performing cortical lesions with a steel needle. Electrode positions were always found between row C–E and arc 1–4 of the barrel cortex.

Following HI, not all animals exhibited cortical injuries in coronal sections alternatively stained for CO and GFAP. We therefore separated individuals for SEP analyses based on the presence of a gliosis scar in the parietal cortex. Rats that presented a gliotic scar as seen as dense zones of GFAP immunofluorescence above the white matter (lesion groups; P10: $n = 15$; P21: $n = 13$) were analyzed separately from the rats without gliosis (no-lesion groups; P10: $n = 8$; P21: $n = 12$). We did not use the criterion of barrel alteration to allocate animals in their respective groups because of its gradual nature. Eleven control rats were recorded at P10 and 14 at P21.

At P10, evoked responses exhibited a negative–positive voltage waveform at contralateral S1 electrodes with onset around 21 ms and lasting more than 200 ms, as illustrated in Figure 3*C*. Upon contralateral stimulation, mean negative and positive peaks were significantly smaller in the right hemisphere of the lesion group as compared with the control and no-lesion groups ($P < 10^{-4}$, unpaired *t*-tests; lesioned: –142.6 ± 34.3 and 81.3 ± 14.1 μV; no-lesion: –262.2 ± 51.6 and 137.7 ± 15.5 μV; control: –320.1 ± 42.2 and 147.1 ± 15.1 μV). In the left hemisphere, the amplitudes of SEP peaks upon contralateral stimulation did not differ between groups (lesioned: –359.2 ± 60.5 and 156.5 ± 22.2 μV; no-lesion: –239.8 ± 51.6 and 118.5 ± 15.5 μV; control: –316.7 ± 27.4 and 158.8 ± 9.1 μV). Accordingly in control and no-lesion groups, SEP peaks were identical in both hemispheres, and the mean SEP ratios calculated between right and left peak-to-peak amplitudes were ≈100%. In contrast, in all the animals of the lesion group,

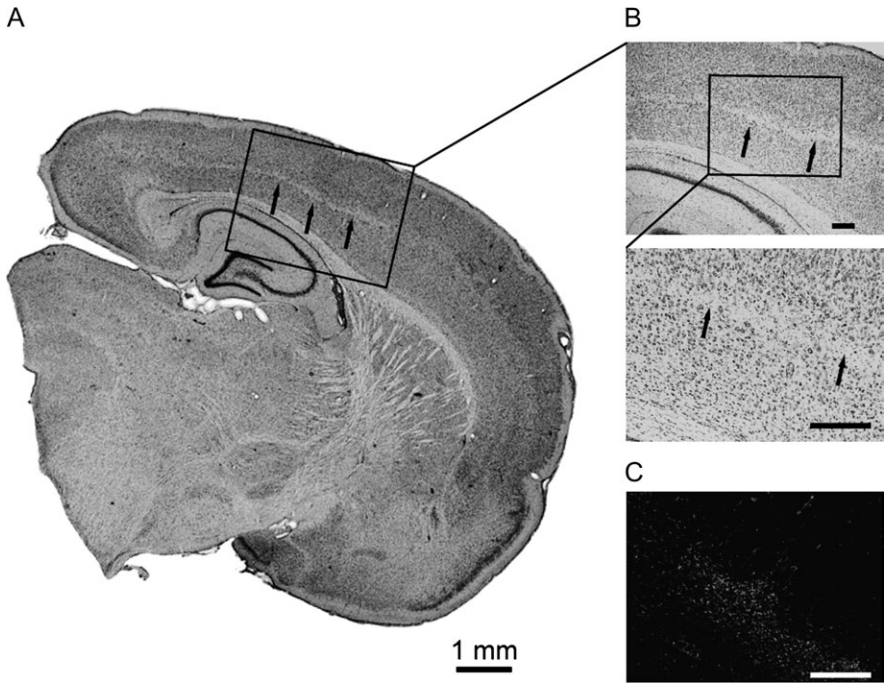

Figure 1. The neonatal HI model. (*A*) Nissl-stained coronal oblique section through the right hemisphere at the level of the parietal cortex in a P21 rat following HI at P3. (*B*) Zones of neuronal loss in infragranular layers (arrows) at higher magnifications. (*C*) GFAP immunostaining from the same region shown on (*B*) note the columnar pattern of dense GFAP staining that characterizes the astrogliosis in infragranular layers of the parietal cortex. Scale bars on (*B* and *C*) are 200 μm.

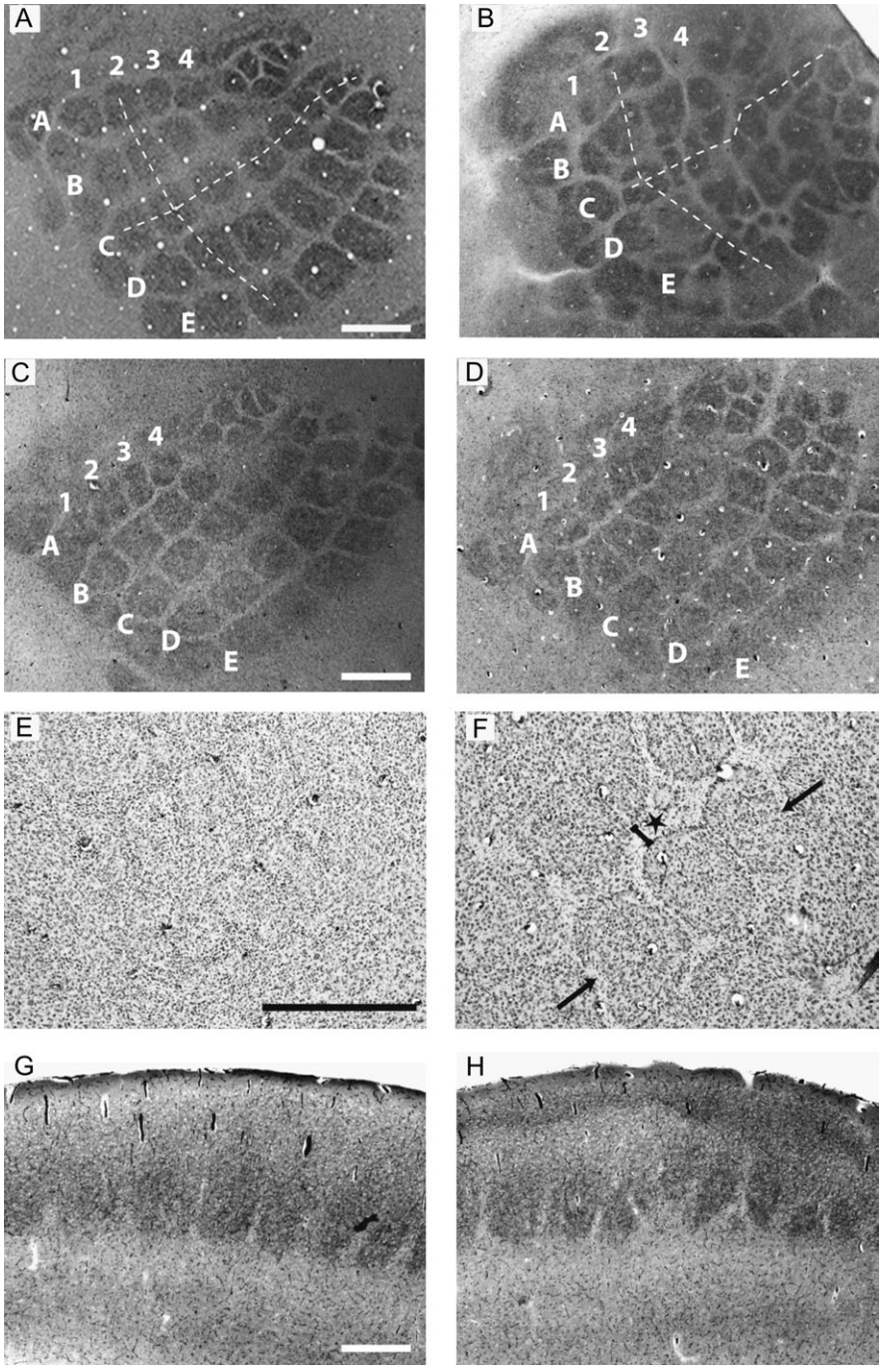

Figure 2. Histomorphological effects of HI in the barrel cortex. (*A*, *B*) Tangential CO sections illustrating the barrel field in the left intact (*A*) and the right injured hemisphere (*B*) from a P21 rat after HI at P3. The barrel morphology and organization in the right S1 cortex are profoundly disrupted. Presumed positions of barrel rows A–E and arcs 1–4 and orientations of row C and arc 2 (dashed lines) are indicated. (*C*, *D*) Tangential CO sections of, respectively, the left and right S1 cortices of a P21 rat illustrating a less severe injury. The morphology of the barrels is slightly altered in the right S1 cortex; however, the barrel rows' organization is still clearly visible. (*E*, *F*) In Nissl-stained sections, the organization of cortical neurons in layer IV of the right hemisphere appears profoundly altered, with enlarged septae (asterisks) and modified barrel's shapes (arrowhead). (*G*, *H*) Coronal CO sections through the left and right S1 cortex of a P21 rat. Barrel shapes are severely altered in the right hemisphere. Scale bars are 300 μm. Note that the orientation of photomicrographs (*B* and *D*) was flipped to facilitate comparisons between barrel fields.

a right/left bias was observed with significantly smaller peak-to-peak amplitudes in the right injured hemisphere than in the left hemisphere ($P < 10^{-5}$, paired *t*-tests) and a mean right/left ratio of 37% HI did not change peak latencies.

At P21, contralateral whisker stimulation evoked a sharp positive–negative wave at 5.5 ms onset and of 30–35 ms duration (Fig. 3*D*). A long-lasting positive period of smaller amplitude followed. Contralateral SEP peaks in the right hemisphere were significantly weaker in the lesion group than in the no-lesion and control groups ($P < 10^{-4}$, unpaired *t*-tests; lesioned: 207.9 ± 38.4 and −166.4 ± 48.6 μV; no-lesion: 536.1 ± 44.4 and −524.7 ± 63.8 μV; control: 543.0 ± 48.0 and −454.2 ± 70.1 μV), whereas no significant differences were observed in the left hemisphere (lesioned: 523.3 ± 57.1 and −396.1 ± 86.5

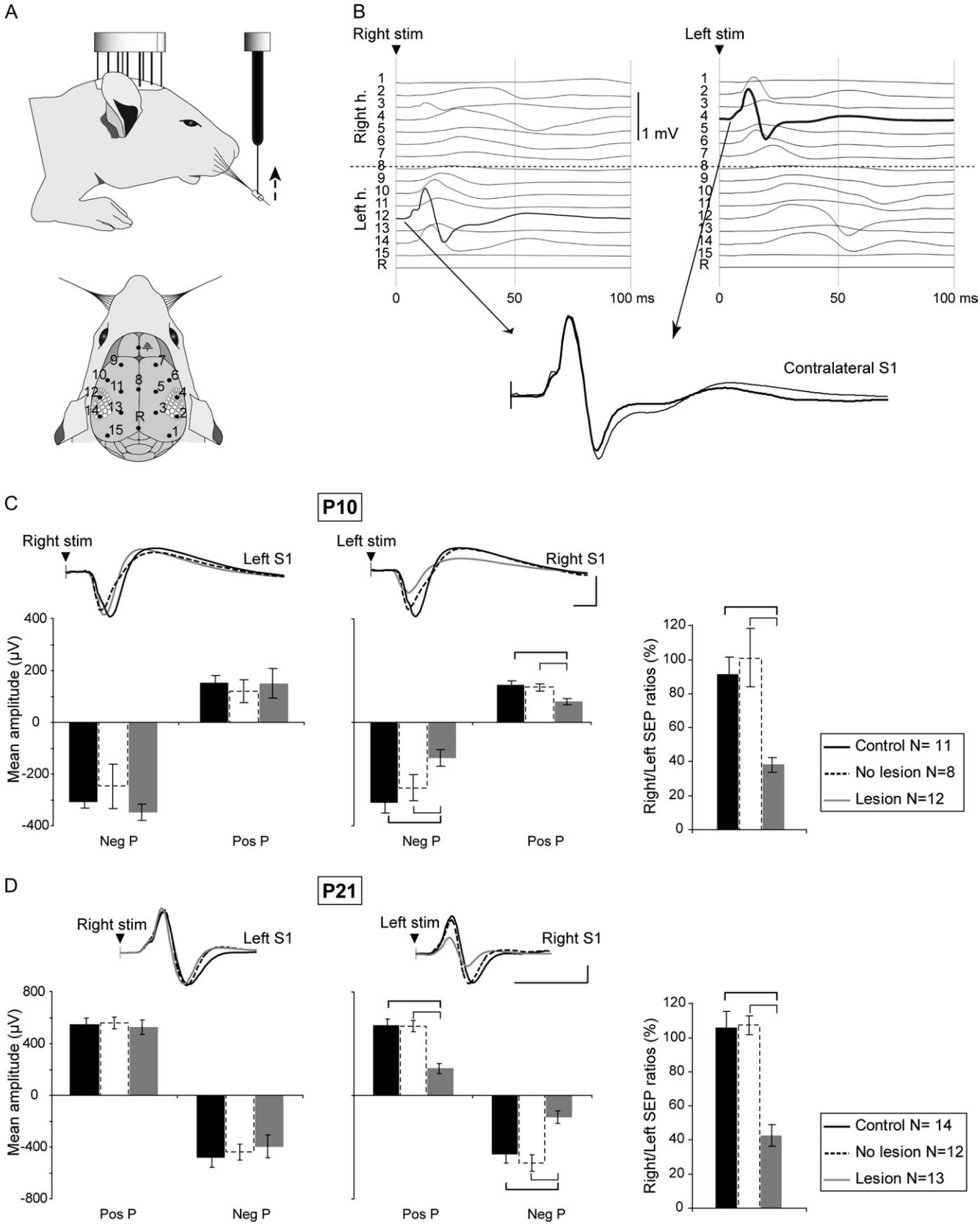

Figure 3. Neonatal HI reduces the contralateral SEP above the injured S1 cortex. (*A*) Under isoflurane anesthesia, 16 stainless steel electrodes are placed in contact with the skull. SEPs are recorded in response to upward deflections of all whiskers on one side of the face. The lower cartoon shows the position of the electrodes on the skull. (*B*) Example of average SEPs recorded in a control animal at P21 for right-sided and left-sided whisker stimulations; numbers next to the traces indicate corresponding electrodes. Superimposed SEPs recorded above the S1 cortex in the left and in the right hemispheres (h.) in response to their respective contralateral whiskers are strictly similar in terms of

μV; no-lesion: 558.3 ± 44.9 and –439.3 ± 60.8 μV; control: 545.9 ± 49.3 and –482.0 ± 75.2 μV). A right/left bias was observed in the animals of the lesion group ($P < 10^{-6}$, paired *t*-tests) with a mean right/left ratio of 42%.

Such a bias in sensory response between hemispheres was present in all lesioned animals; however, its degree was related to the importance of the lesion. We quantified this effect in the P21 lesioned group by comparing SEP right/left ratios to a morphological index of the cortical lesion in each animal. This index was calculated as the right/left ratio of cortical gray matter surfaces measured on a Nissl-stained coronal section of the S1 cortex between the rhinal sulcus and the cingulum in both hemispheres (Sizonenko et al. 2003). The obtained mean surface ratio was 77.8%, similar to the values previously reported by Sizonenko et al. (2003). SEP ratios and surface ratios were significantly correlated (Pearson test correlation: R^2 = 0.51, P = 0.006), suggesting that the stronger the morphological injury the greater the physiological deficit.

Using multichannel intracortical recordings of LFP and CSD calculations, we further analyzed in P21 rats how the HI injury altered the laminar pattern of somatosensory responses in the barrel cortex. Whisker-evoked cortical activation started with a current sink in layer IV rapidly invading layers II and III and concomitant with superficial and deep sources (Fig. 4*A*). A large source then replaced the initial sink in layers II and III, whereas sinks took place in the superficial layer and in layer V. Although this pattern was partially preserved in the lesioned cortex, several alterations were observed. First, the amplitude of the evoked currents was smaller during the entire response and along all the length of the vertical axis. Second, the deep source was evoked more superficially in lesioned (1400–1700 μm) than in control rats (1000–1400 μm). Figure 4*B* presents grand average traces at selected electrodes from 4 control and 4 lesioned animals, illustrating the general decrease in amplitude following HI.

Deficit and Recovery of the Large-Scale SEP Processing in Sensorimotor Networks

Whisker deflection produces heterogeneous waveforms over wide regions of the epicranial surface reflecting activation of large-scale networks. We used topographic pattern analyses derived from human evoked potential studies (Michel et al. 2004; Mégevand et al. 2008) to investigate further the data of the control and lesion groups. At P10, 4 component maps were identified by cluster analysis of the grand average SEPs in the control and lesion groups (Fig. 5*A*,*B*). In both groups, the SEP began with a focal negativity over the contralateral somatosensory parietal cortex at 23 ms onset followed by a positivity around 30 ms later. During this second map, activity also invaded frontal regions at coordinates corresponding to the location of the motor cortex (M1) in the adult rat (Hall and Lindholm 1974; Huntley 1997; Hoffer et al. 2003). Evoked activity over the hemisphere ipsilateral to the stimulus remained almost negligible. A pointwise *t*-test procedure on all electrodes revealed lower evoked voltages over both parietal and frontal regions contralateral to the stimulus during almost the entire duration of the response in the lesion group. To confirm observations from multiple *t*-tests with a robust global statistical comparison, we applied a nonparametric randomization procedure to map topographies, which revealed significant differences between groups from 41 to 60, 82 to 104, and 179 to 190 ms poststimulus (Fig. 5*C*). During these periods, significant lower voltages were found at both parietal and frontal regions contralateral to the stimulation, as illustrated with the interpolated *t* maps calculated by averaging the 1 – *P* values from the pointwise *t*-tests along these time windows.

At P21, SEPs had considerably evolved: evoked responses are faster, shorter, and invade wider areas (Fig. 6*A*,*B*). In both the control and lesion groups, it started with a focal positivity above the contralateral somatosensory parietal cortex at 7 ms onset. Ten milliseconds later, it was replaced by a focal negativity, whereas a positive deflection invaded the frontal region as well as the parietal region of the opposite hemisphere where it subsequently spread above the frontal region. The pointwise *t*-tests indicated that significant differences between groups were limited to parietal electrodes contralateral to the stimulus (E2–4; Fig. 6*C*). The spatial analysis of map topographies confirmed significant differences during 2 periods between 12 and 17 ms and 19 and 30 ms poststimulus (Fig. 6*C*). To conclude, significant voltage alterations were spatially restricted to the somatosensory region contralateral to the stimulus at P21, as illustrated by the *t* maps.

The absence of deficit at frontal regions in P21 animals could suggest that a functional recovery process took place in the sensory–motor networks between P10 and P21. To confirm these observations, we looked at the evolution of the SEP across time in the same animals using a supplementary longitudinal batch of rats, either control (n = 6; L-control group) or HI injured (n = 5; L-lesion group). We here focused on voltage signals recorded at center electrodes above the somatosensory and motor regions (E4 and E12, E7 and E9; right and left hemisphere, respectively). SEP peaks were significantly decreased in the L-lesion group as compared with control at the level of the injured somatosensory cortex at both P10 (Fig. 7; L-lesioned: –136.5 ± 29.3 and 75.1 ± 18.9 μV; L-control: –274.6 ± 54.3 and 120.3 ± 22.8 μV) and P21 (L-lesioned: 215.1 ± 46.8 and –205.3 ± 94.2 μV; L-control: 502.1 ± 91.3 and –445.9 ± 149.6 μV). Interestingly, the right/left ratio significantly increased from P10 to P21 in lesioned animals (mean: 34% vs. 58%; $P < 0.01$; paired *t*-test). This was not due to modified responses in the left hemisphere as left SEPs were not different in lesioned and control animals at any ages (data not shown). At the level of the motor cortex, peak amplitudes were reduced at P10 in the lesioned group as compared with control (lesioned: –28.5 ± 7.6 and 27.4 ± 7.3 μV; control: –47.8 ± 14.2 and 34.5 ± 10.7 μV) without reaching statistical significance, which should be due to the variability of voltage values and the small size of our population. However, measurements of relative amplitudes using right/left ratio revealed significantly lower contralateral motor responses in the right hemisphere as compared with the

timing and amplitude (average ± standard error of the mean [SEM] of 50 traces). (*C*) Grand average traces of the SEPs recorded above the left and right S1 cortices in response to respective contralateral stimulations in control, no-lesion, and lesion groups of P10 rats. Below, corresponding histograms show the mean ± SEM amplitude quantifications for the negative (Neg *P*) and positive (Pos *P*) peaks of the SEP. The bar graph on the right shows the mean right/left ratios of the peak-to-peak amplitudes in the 3 groups. (*D*) Similarly, grand average traces, mean SEP peaks, and mean right/left ratios of the peak-to-peak amplitudes measured in control, no-lesion, and lesion groups of P21 rats. Note that time and amplitude scales are different at P10 and P21. At both age, SEP peaks are greatly reduced in the right hemisphere of the lesion groups as compared with peaks of the control and no-lesion groups. Scale bars are 50 ms and 200 μV; brackets indicate significant differences at $P < 0.001$.

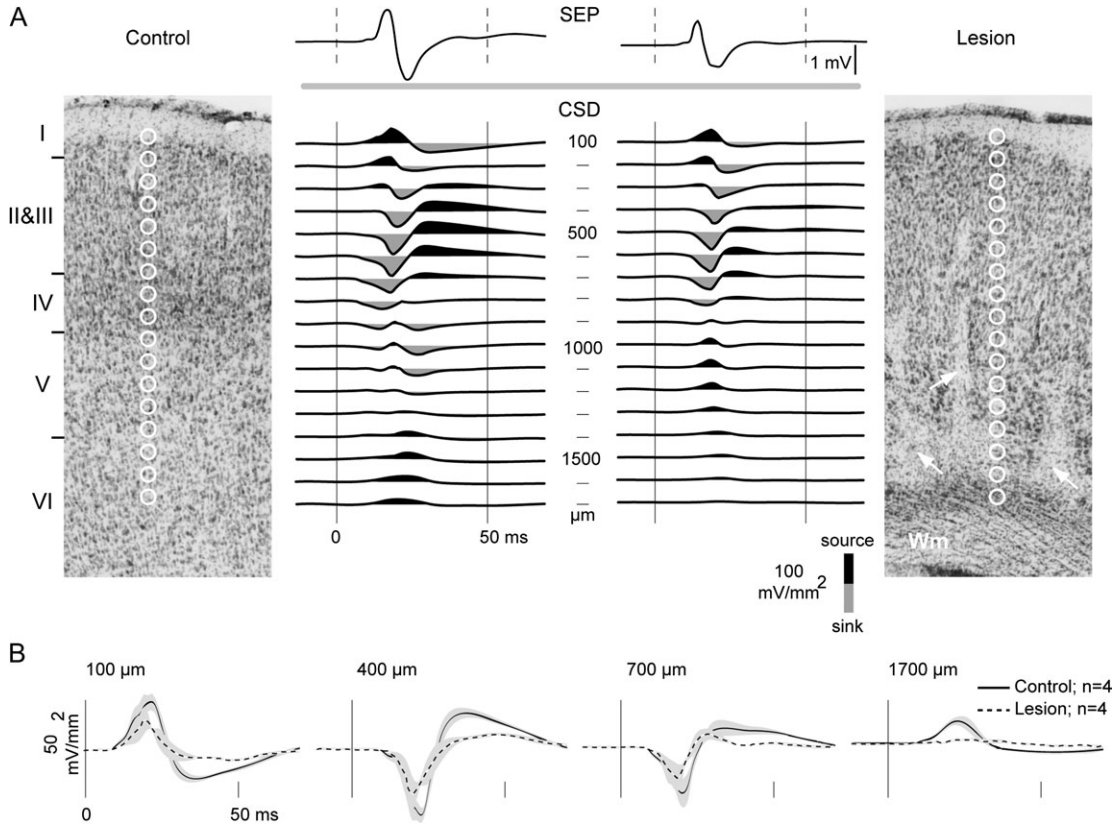

Figure 4. Intracortical recordings in the lesion S1 cortex. (*A*) Average SEPs and CSDs recorded at the right S1 cortices of 1 control (left) and 1 lesion (right) P21 animal in response to 50 stimulations of contralateral whiskers. Current sinks are colored in black, sources in gray. Under isoflurane anesthesia, epicranial SEPs were recorded first and then a craniotomy was realized to process to intracortical recordings beneath the former position of the epicranial electrode. The localization of the intracortical electrodes (white circles) on the Nissl-stained coronal sections presented next to the corresponding traces was inferred from Chicago blue injections realized after the recording session. Arrowheads in the lesion's photomicrograph point to zones of neuronal loss (WM: white matter). Approximate limits of cortical layers are indicated next to the control's photomicrograph. (*B*) Average CSD traces and standard error of the mean (gray background) of 4 control and 4 lesioned animals at P21 at 4 selected depth: 100, 400, 700, and 1700 µm.

left hemisphere, with a mean negative bias for responses in the right hemisphere of 57% ($P < 0.01$; paired *t*-test). At P21, the amplitude of the SEP evoked at the right motor cortex was not altered as compared with control (L-lesioned: 95.3 ± 20.1 and −82.2 ± 16.3 µV; L-control: 119.8 ± 21.9 and −90.8 ± 33.8 µV), and no interhemispheric bias was detected any more, confirming the observations made with the nonlongitudinal groups.

Discussion

Previous studies established that a moderate HI in the rat at P3 results in selective neuronal damage and persistent gliosis in the parietal cortex (Sizonenko et al. 2003, 2007). Here, we demonstrate that the ischemic damage leads to malformations of the somatosensory barrel field in the S1 cortex. These changes are paralleled by discrete, spatially distributed changes in evoked potential maps in somatosensory–motor networks. In particular, our results indicate that at P10, the amplitudes of SEPs recorded over the sensory parietal and motor frontal regions are significantly reduced after HI. However, at P21, the deficit in SEP amplitude is restricted to the injured barrel cortex, suggesting that a functional recovery process took place in sensorimotor networks.

Neonatal HI Injury Alters Barrel Field Organization

An important aspect of neonatal injuries is their regional specificity (Volpe 2009). The characteristic pattern of injury in the HI model at P3 involves neuronal loss mainly infragranular layers of the parietal cortex (Sizonenko et al. 2003, 2005). We do not have a clear explanation for this regional specificity. This phenomenon may be related to the specificity of local vascular supply and the immaturity of the penetrator vessels from superficial arteries (Rorke 1992). The maturation pattern of the excitatory synaptic network in infragranular layers might also contribute to the vulnerability of this region to ischemic lesions. Earlier work in rodents demonstrated that peripheral interventions including plucking whiskers, cauterizing follicles, and disrupting sensory nerves from whiskers could alter the organization of barrels and modify CO staining (Van der Loos and Woolsey 1973; Killackey et al. 1976; Dietrich et al. 1981). Central lesions involving the barrel field such as aspiration of the cortex (Finger et al. 1978) or transcranial freeze lesion (Jacobs et al. 1999) at P0 were shown to disrupt barrel field pattern. Our results show for the first time that HI injury at P3 leads to disorganized overall barrel pattern as observed in both CO- and Nissl-stained sections. The structural abnormalities showed some variability from one animal to the other. These include no visible alterations of the barrel structures, irregularly shaped and spaced barrels, fusion of barrels, or their complete absence. This interindividual variability in pathological changes in the barrel cortex likely corresponds to the different degree of ischemic lesions (Sizonenko et al. 2003, 2005).

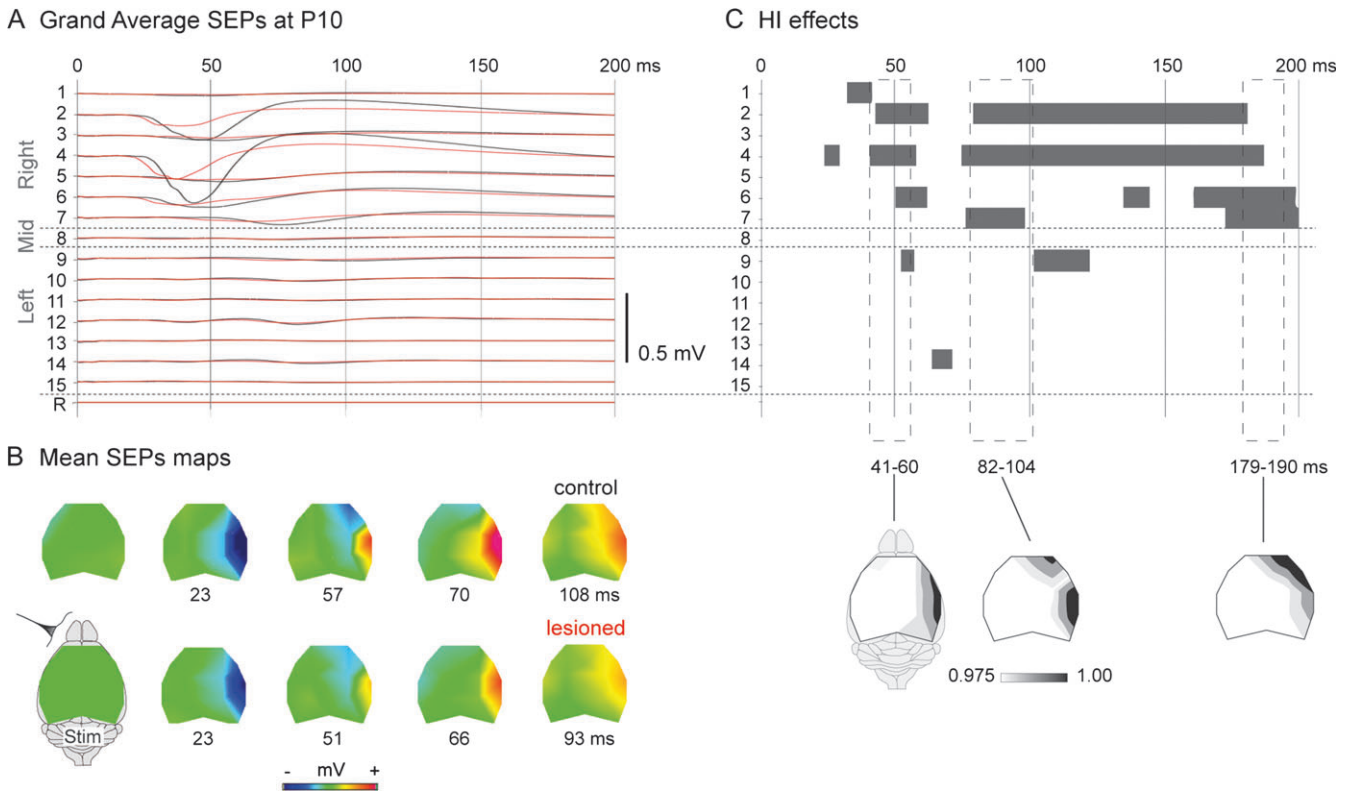

Figure 5. Effects of HI on the SEP topographies at P10. (*A*) Grand average waveforms of the SEPs from 0 to 200 ms poststimulation of left whiskers in the control and lesion groups. (*B*) Mean topographic maps identified by the cluster analysis of the grand averages. Mean times of occurrence of these maps, calculated by fitting them back to the data from individuals in each group as previously described (Mégevand et al. 2008), are indicated. (*C*) Pointwise *t*-tests between the control and lesion groups: gray bars indicate at each electrode periods during which *P* values were significant for at least 5 ms consecutively (unpaired *t*-test at $P < 0.05$). Dashed boxes indicate episodes of significant topographic differences between groups as revealed by a randomization procedure on spatial dissimilarity. Below, topographic maps of the significant voltage differences calculated by averaging $1 - P$ values from the pointwise *t*-tests during the periods of significant topographic differences.

Several mechanisms could contribute to these morphological alterations. Disrupted barrel organization could be the consequence of simple displacement of barrels due to different degrees of cortical atrophy after the ischemic lesion. Although we cannot exclude this possibility, based on the irregular shape and spacing of barrels, this mechanism would not explain the pathological changes. It is also possible that the ischemic injury directly involved the neuronal population in layer IV. Although the lesion mainly alters infragranular layers, sometimes columnar patches of neuronal degeneration and astrogliosis were observed in layer IV (Sizonenko et al. 2003, 2005). In rats, CO-stained barrels contain high density of TC terminals from ventral posterior medial (VPM), whereas CO-light regions within septae and between subbarrel domains are enriched in cell somata and in myelinated axons (Land and Erickson 2005). The altered CO-stained barrel shapes and increased interbarrel spaces devoid of Nissl staining could suggest a reduced density of both layer IV neurons and TC terminals.

In both rats and mice, the typical clustering of cortical neurons in individual barrel structures and the patterning of their TC terminal counterparts are not apparent before P3 (Rice and Van der Loos 1977; Erzurumlu et al. 1990; Schlaggar and O'Leary 1994; Margret et al. 2006). TC axon terminals from the VPM and posterior medial (POm) nuclei are present in layer IV at P3, but their respective clustering in barrel domain and localization to septae are not fully mature (Wise and Jones 1978; Erzurumlu and Jhaveri 1990; Catalano et al. 1991; Kichula and Huntley 2008). It has been repeatedly demonstrated that these cortical developmental processes crucially depend on input activity. Destruction of whisker follicles or sectioning of the infraorbital branch of the trigeminal nerve between P0 and P6 disrupts the normal segregation of TC terminals (Jensen and Killackey 1987) and the development of cytoarchitectonic barrel structures (Van der Loos and Woolsey 1973; Harris and Woolsey 1981). Maximal perturbations occur with lesions done at P0, then become gradually less severe, and disappear after P6 (Rice and Van der Loos 1977; Jeanmonod et al. 1981; Mccasland et al. 1992). These effects are dependent on cortical activity; however, blocking postsynaptic activity in the cortex per se does not damage the barrel patterning (Schlaggar et al. 1993). It is thus possible that the HI lesion performed during this critical period could cause a significant and nonhomogeneous degeneration of TC afferents in the subplate and infragranular layers and interfere with the normal maturation of the TC terminals in barrel domains.

Neonatal Development of SEPs from P10 to P21

SEP responses recorded at P10 and P21 were different in at least 3 aspects. First, responses have longer onset latency and duration and lower amplitudes at P10 than at P21, as expected from intracortical recordings and voltage or calcium-sensitive dye imaging studies showing that whisker-evoked responses in the immature rodents are slower and weaker than in adults (Stern et al. 2001; Borgdorff et al. 2007). SEP in human newborns similarly exhibit radical changes in latency, duration, and amplitude during the first weeks of life (Pihko and

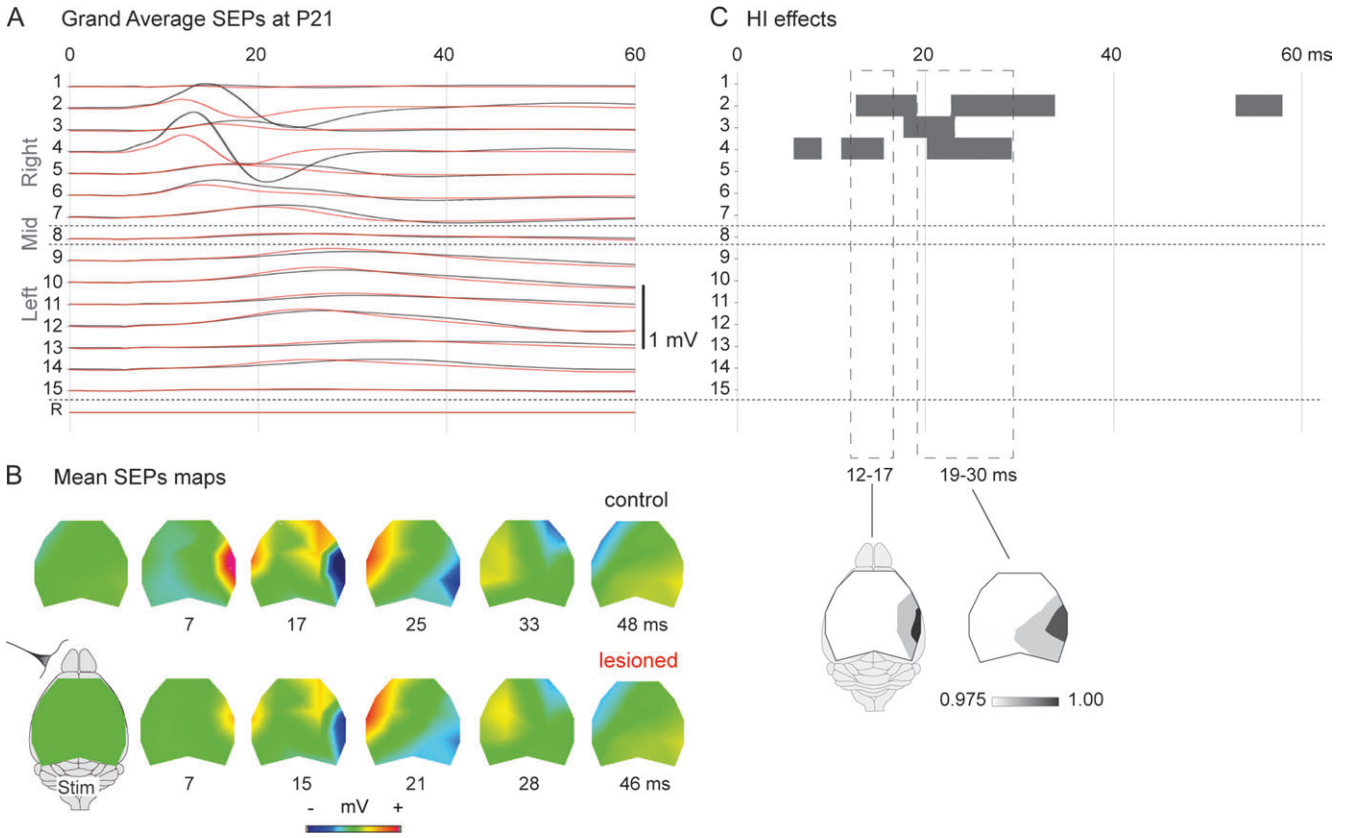

Figure 6. Effects of HI on the SEP topographies at P21. (*A*) Grand average waveforms of the SEPs from 0 to 80 ms poststimulation of left whiskers in the control and lesion groups. (*B*) Topographic maps with mean times of occurrence. (*C*) Periods of significant *t*-test values at each electrode (gray bars; unpaired *t*-test at $P<0.05$) and topographic dissimilarity between the control and lesion groups (dashed boxes; randomization procedure). Below, maps of the significant voltage differences at each electrode between groups during the periods of significant differences in map topographies ($1-P$).

Lauronen 2004). Second, the SEP waveform recorded above the barrel cortex begins with a negative–positive wave at P10 instead of the characteristic early positive–negative deflection observed at P21 (the present study) in adult mice (Troncoso et al. 2000) and in rat epipial recordings (Barth et al. 1994). Such a shift in polarity of surface voltage components between immature and mature SEP has not yet been thoroughly documented in rodents (Thairu 1971). It has been observed in premature human newborns (Vanhatalo and Lauronen 2006), suggesting that, although the underlying mechanisms remain unknown, the functional cortical development of the P10 rat is highly immature.

Third, topographical analyses revealed differences in large-scale sensorimotor networks. At P21, whisker deflection evokes widely distributed responses, invading sequentially the parietal sensory and frontal motor regions of the contralateral than ipsilateral hemisphere. Whisker-evoked activations in sensory and motor areas of both hemispheres were previously described in adult rats, although these recordings were not made simultaneously (Carvell and Simons 1987; Barth et al. 1994; Farkas et al. 1999; Brett-Green et al. 2004; Ahrens and Kleinfeld 2004), and mice (Ferezou et al. 2007; Mégevand et al. 2008). This distributed processing of sensory-evoked activity across multiple cortical networks should allow sensorimotor integration as well as interhemispheric spatial correlation of inputs. Cortico-cortical projections from S1 and TC projections from POm to the motor cortex (Izraeli and Porter 1995; Hoffer et al. 2003, 2005) and reciprocal commissural fibers between somatosensory cortices (Olavarria et al. 1984; Hayama and Ogawa 1997) likely constitute the structural basis for the described flow of evoked activity. At P10, however, evoked activity is less distributed, and almost no response can be detected in the hemisphere ipsilateral to the stimulated whiskers. This could be explained by the immaturity of intracortical synaptic circuitry (Foeller and Feldman 2004) and the incomplete myelinization of long axonal and callosal projections (Fields 2005; Jito et al. 2008).

Deficit and Recovery of Evoked Response within Developing Sensorimotor Networks

After neonatal HI, the amplitude of the contralateral SEP recorded at P10 and at P21 is strongly reduced in the somatosensory area of the injured hemisphere, whereas no changes were observed in the noninjured hemisphere, leading to a right/left bias. Intracortical recordings in injured S1 at P21 point to a general decrease of evoked responses in all cortical layers. The strongest changes are observed in infragranular layers where the late sink is almost absent, in agreement with the main location of the gliotic scar and the patches of neuronal loss. The lesser extent of cortical activation along the vertical axis is likely due to the reduction in cortical thickness because the 1–3 lowermost electrodes were sometimes located beneath the cortex in the white matter. It should be noted that despite the reduced cortical thickness, we never observed subdural or epidural ischemic spaces beneath the parietal bone, the development of the skull following that of the brain. This is

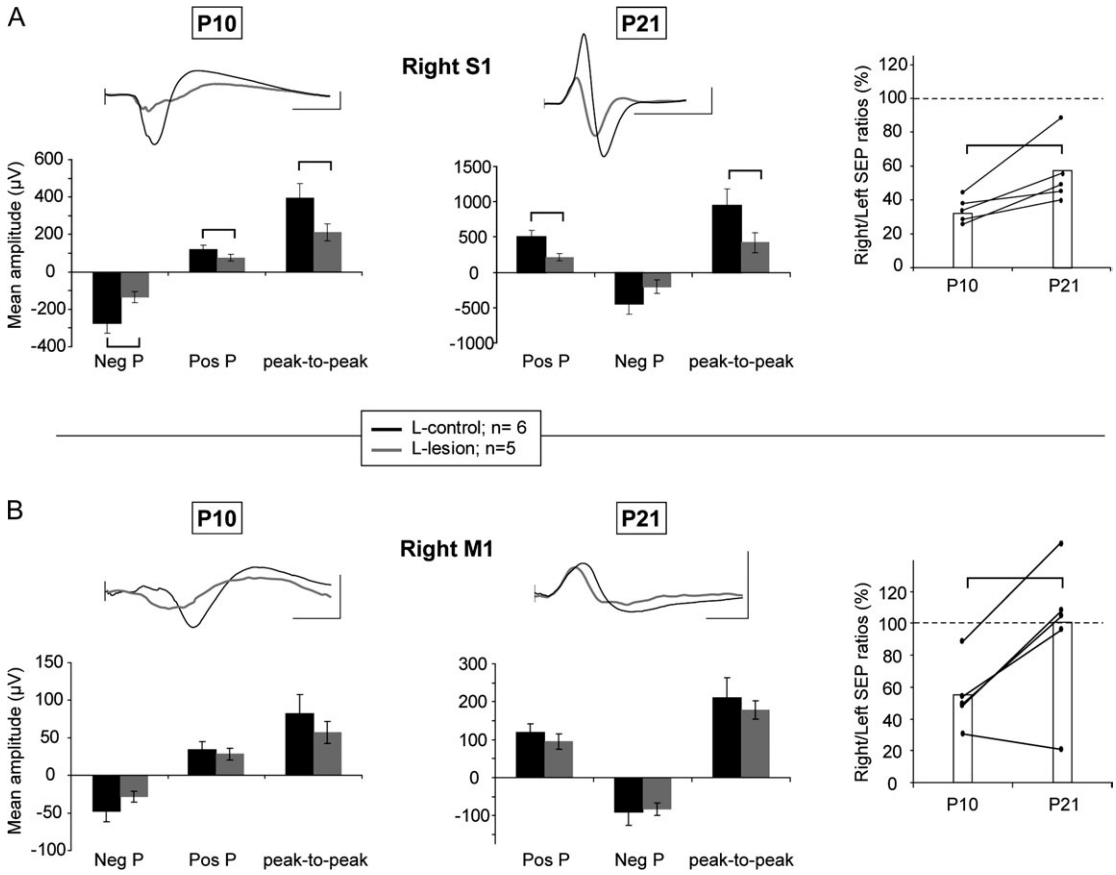

Figure 7. SEP peaks at somatosensory parietal and motor frontal electrodes in longitudinal groups. Mean ± standard error of the mean amplitudes of the positive and negative SEP peaks recorded above the right parietal electrode 12 (*A*, right S1) and the frontal cortex electrode 7 (*B*, right M1) at P10 and at P21 in longitudinal lesioned animals (L-lesion) and longitudinal control (L-control). Note that time and amplitude scales are different at P10 and P21. On the right side, mean ratio of the peak-to-peak amplitudes together with individual values (dots) at P10 and at P21; a line is traced between recordings made in the same animal at both ages. Brackets indicate significant differences at $P < 0.01$. Scale bars are 50 ms and 100 μV at P10 and 20 ms and 200 μV at P21.

crucial because the amplitude of voltages recorded at the skull surface depends on the conduction properties of the tissues in which currents flow. The reduction in voltages recorded at the skull surface most likely reflects neuronal loss and disorganization in the primary cortex, reducing the "power" of the intracortical generator of epicranial signals.

In the longitudinal study, paired statistics put into light a significant decrease in the right/left bias from P10 to P21, suggesting that at least a partial functional recovery from the HI effects could occur at the level of the lesioned somatosensory cortex. It is possible that the injured hemisphere recovers at P21 from some acute effects of the lesion still affecting S1 at P10, such as edema, altered blood supply, or other reversible ischemic damages (Witte et al. 2000). Postlesional cortical plasticity could also be engaged (Dijkhuizen et al. 2001), particularly at layer IV–layers II and III connections that mature around P10–P15 and are highly plastic during this critical period (Foeller and Feldman 2004).

Sensory-evoked activity in the cortex crucially depends upon the S1 area contralateral to the stimulus, as inactivation of this area abolishes all cortical responses (Farkas et al. 1999; Shuler et al. 2001). Accordingly, topographical SEP analyses at P10 detected differences between control and lesioned rats in both the lesioned S1 and in the motor frontal area of the same hemisphere. However, these changes are transient in the motor area; at P21, changes only concern the contralateral S1. Although responses differ widely and cannot be compared directly between P10 and P21, we demonstrate here using nonlongitudinal and longitudinal recordings and right/left interhemispheric ratio that the amplitude of the epicranial SEP recovers completely in the motor area. These results strongly suggest that a process of functional recovery may take place in the sensory–motor functional networks between P10 and P21.

Not only do evoked responses apparently recover in the motor area but also further ipsilateral-evoked activity in sensorimotor regions of the noninjured hemisphere is not altered at P21, as compared with controls. HI effects on ipsilateral responses cannot be tested at P10 because those were almost not detectable at this age. One could hypothesize that a reduction in response amplitude in S1 would have led to a fainter output toward networks in the motor cortex of the same hemisphere as well as in the opposite hemisphere and consequently result in a reduction in amplitude of evoked epicranial responses in those regions. The observation that SEPs are not altered in these downstream networks at P21 is intriguing. One possibility is that changes in the intrinsic excitability of motor cortical networks remote from the HI injury allow a functional adaptation to weaker inputs from the lesioned S1. Functional adaptations after stroke have been

associated with cortical plasticity mechanisms in adult rats (Nudo 2006). This could even be facilitated here by the fact that intracortical circuits are still engaged in a process of postnatal maturation during the first weeks of life and exhibit greater plasticity than in adulthood (Micheva and Beaulieu 1996; Lendvai et al. 2000; Bender et al. 2003). It could be also that the supragranular layers of S1, apparently unaltered by the HI lesion, maintain a powerful output to other cortical regions; however, this is not suggested by intracortical recordings that revealed a general decrease of evoked activity in all layers.

In conclusion, we demonstrated that neonatal HI injury results in disruption of barrel cortex organization in the rat. Analyzing the spatiotemporal dynamics of postlesion functional plasticity, we showed that in addition to the clear-cut deficit in evoked responses in the barrel cortex, discrete changes occur in large-scale somatosensory–motor networks including the motor cortex that may underlie functional recovery. Importantly, the surface potential mapping we used in this study represents macroscopic approaches, characteristic of noninvasive brain studies in humans. Thus, combining this methodology with a rat/mouse model opens new possibilities to compare animal recordings with human EEG recordings and cognitive development and to investigate phenomenologies provided by human studies at the cellular and molecular levels.

Funding

Swiss National Science Foundation (31003A-112233 to S.V.S., 320000-111783 to C.M.M., 323600-111505 to P.M., 3100A0-116613/1 to J.Z.K.); Meissner Foundation to C.Q. and J.Z.K.; European Community Grant Promemoria (512012-2005 to J.Z.K.).

Notes

We thank Cynthia Saadi for technical assistance with the histological preparations. The Cartool software (http://brainmapping.unige.ch/Cartool.php) is developed by Denis Brunet from the Functional Brain Mapping Laboratory, Geneva, supported by the Center for Biomedical Imaging, Geneva and Lausanne, Switzerland. *Conflict of Interest*: None declared.

Address correspondence to Dr Charles Quairiaux, Department of Neurosciences, University of Geneva, CMU Rue Michel-Servet 1, CH-1211 Geneva 4, Switzerland. Email: charles.quairiaux@unige.ch.

References

Ahrens KF, Kleinfeld D. 2004. Current flow in vibrissa motor cortex can phase-lock with exploratory rhythmic whisking in rat. J Neurophysiol. 92:1700–1707.

Armstrong-James M, Fox K. 1987. Spatiotemporal convergence and divergence in the rat S1 "barrel" cortex. J Comp Neurol. 263:265–281.

Barth DS, Kithas J, Di S. 1994. The anatomic organization of evoked potentials in rat parietal cortex: electrically evoked commissural responses. J Neurophysiol. 72:139–149.

Bender KJ, Rangel J, Feldman DE. 2003. Development of columnar topography in the excitatory layer 4 to layer 2/3 projection in rat barrel cortex. J Neurosci. 23:8759–8770.

Borgdorff AJ, Poulet JF, Petersen CC. 2007. Facilitating sensory responses in developing mouse somatosensory barrel cortex. J Neurophysiol. 97:2992–3003.

Brett-Green B, Paulsen M, Staba RJ, Fifkova E, Barth DS. 2004. Two distinct regions of secondary somatosensory cortex in the rat: topographical organization and multisensory responses. J Neurophysiol. 91:1327–1336.

Carmichael ST. 2005. Rodent models of focal stroke: size, mechanism, and purpose. NeuroRx. 2:396–409.

Carvell GE, Simons DJ. 1987. Thalamic and corticocortical connections of the second somatic sensory area of the mouse. J Comp Neurol. 265:409–427.

Catalano SM, Robertson RT, Killackey HP. 1991. Early ingrowth of thalamocortical afferents to the neocortex of the prenatal rat. Proc Natl Acad Sci USA. 88:2999–3003.

Clancy B, Darlington RB, Finlay BL. 2001. Translating developmental time across mammalian species. Neuroscience. 105:7–17.

Craig A, Ling LN, Beardsley DJ, Wingate-Pearse N, Walker DW, Hohimer AR, Back SA. 2003. Quantitative analysis of perinatal rodent oligodendrocyte lineage progression and its correlation with human. Exp Neurol. 181:231–240.

Dietrich WD, Durham D, Lowry OH, Woolsey TA. 1981. Quantitative histochemical effects of whisker damage on single identified cortical barrels in the adult mouse. J Neurosci. 1:929–935.

Dijkhuizen RM, Ren J, Mandeville JB, Wu O, Ozdag FM, Moskowitz MA, Rosen BR, Finklestein SP. 2001. Functional magnetic resonance imaging of reorganization in rat brain after stroke. Proc Natl Acad Sci USA. 98:12766–12771.

Erzurumlu RS, Jhaveri S. 1990. Thalamic axons confer a blueprint of the sensory periphery onto the developing rat somatosensory cortex. Brain Res Dev Brain Res. 56:229–234.

Erzurumlu RS, Jhaveri S, Benowitz LI. 1990. Transient patterns of Gap-43 expression during the formation of barrels in the rat somatosensory cortex. J Comp Neurol. 292:443–456.

Farkas T, Kis Z, Toldi J, Wolff JR. 1999. Activation of the primary motor cortex by somatosensory stimulation in adult rats is mediated mainly by associational connections from the somatosensory cortex. Neuroscience. 90:353–361.

Ferezou I, Haiss F, Gentet LJ, Aronoff R, Weber B, Petersen CC. 2007. Spatiotemporal dynamics of cortical sensorimotor integration in behaving mice. Neuron. 56:907–923.

Ferriero DM. 2004. Neonatal brain injury. N Engl J Med. 351:1985–1995.

Fields RD. 2005. Myelination: an overlooked mechanism of synaptic plasticity? Neuroscientist. 11:528–531.

Finger S, Simons D, Posner R. 1978. Anatomical, physiological, and behavioral effects of neonatal sensorimotor cortex ablation in the rat. Exp Neurol. 60:347–373.

Foeller E, Feldman DE. 2004. Synaptic basis for developmental plasticity in somatosensory cortex. Curr Opin Neurobiol. 14:89–95.

Fox K. 2002. Anatomical pathways and molecular mechanisms for plasticity in the barrel cortex. Neuroscience. 111:799–814.

Frostig RD. 2006. Functional organization and plasticity in the adult rat barrel cortex: moving out-of-the-box. Curr Opin Neurobiol. 16:445–450.

Hall RD, Lindholm EP. 1974. Organization of motor and somatosensory neocortex in the albino rat. Brain Res. 66:23–38.

Harris RM, Woolsey TA. 1981. Dendritic plasticity in mouse barrel cortex following postnatal vibrissa follicle damage. J Comp Neurol. 196:357–376.

Hayama T, Ogawa H. 1997. Regional differences of callosal connections in the granular zones of the primary somatosensory cortex in rats. Brain Res Bull. 43:341–347.

Hoffer ZS, Arantes HB, Roth RL, Alloway KD. 2005. Functional circuits mediating sensorimotor integration: quantitative comparisons of projections from rodent barrel cortex to primary motor cortex, neostriatum, superior colliculus, and the pons. J Comp Neurol. 488:82–100.

Hoffer ZS, Hoover JE, Alloway KD. 2003. Sensorimotor corticocortical projections from rat barrel cortex have an anisotropic organization that facilitates integration of inputs from whiskers in the same row. J Comp Neurol. 466:525–544.

Huntley GW. 1997. Differential effects of abnormal tactile experience on shaping representation patterns in developing and adult motor cortex. J Neurosci. 17:9220–9232.

Inder TE, Huppi PS, Warfield S, Kikinis R, Zientara GP, Barnes PD, Jolesz F, Volpe JJ. 1999. Periventricular white matter injury in the premature infant is followed by reduced cerebral cortical gray matter volume at term. Ann Neurol. 46:755–760.

Inder TE, Warfield SK, Wang H, Huppi PS, Volpe JJ. 2005. Abnormal cerebral structure is present at term in premature infants. Pediatrics. 115:286–294.
Izraeli R, Porter LL. 1995. Vibrissal motor cortex in the rat: connections with the barrel field. Exp Brain Res. 104:41–54.
Jacobs KM, Mogensen M, Warren E, Prince DA. 1999. Experimental microgyri disrupt the barrel field pattern in rat somatosensory cortex. Cereb Cortex. 9:733–744.
Jeanmonod D, Rice FL, Van der Loos H. 1981. Mouse somatosensory cortex—alterations in the barrelfield following receptor injury at different early postnatal ages. Neuroscience. 6:1503–1535.
Jenkins WM, Merzenich MM. 1987. Reorganization of neocortical representations after brain injury: a neurophysiological model of the bases of recovery from stroke. Prog Brain Res. 71:249–266.
Jensen KF, Killackey HP. 1987. Terminal arbors of axons projecting to the somatosensory cortex of the adult rat. II. The altered morphology of TC afferents following neonatal infraorbital nerve cut. J Neurosci. 7:3544–3553.
Jito J, Nakasu S, Ito R, Fukami T, Morikawa S, Inubushi T. 2008. Maturational changes in diffusion anisotropy in the rat corpus callosum: comparison with quantitative histological evaluation. J Magn Reson Imaging. 28:847–854.
Kichula EA, Huntley GW. 2008. Developmental and comparative aspects of posterior medial thalamocortical innervation of the barrel cortex in mice and rats. J Comp Neurol. 509:239–258.
Killackey HP. 1973. Anatomical evidence for cortical subdivisions based on vertically discrete thalamic projections from ventral posterior nucleus to cortical barrels in rat. Brain Res. 51:326–331.
Killackey HP, Belford G, Ryugo R, Ryugo DK. 1976. Anomalous organization of thalamocortical projections consequent to vibrissae removal in newborn rat and mouse. Brain Res. 104:309–315.
Land PW, Erickson SL. 2005. Subbarrel domains in rat somatosensory (S1) cortex. J Comp Neurol. 490:414–426.
Lendvai B, Stern EA, Chen B, Svoboda K. 2000. Experience-dependent plasticity of dendritic spines in the developing rat barrel cortex in vivo. Nature. 404:876–881.
Leung L-WS. 1990. Field potentials in the central nervous system: recording, analysis, and modeling. In: Boulton AA, Baker GB, Vanderwolf CH, editors. Neurophysiological techniques, II. Applications to neural systems. Clifton, NJ: Humana Press. p. 277–312.
Margret CP, Li CX, Chappell TD, Elberger AJ, Matta SG, Waters RS. 2006. Prenatal alcohol exposure delays the development of the cortical barrel field in neonatal rats. Exp Brain Res. 172:1–13.
Mccasland JS, Bernardo KL, Probst KL, Woolsey TA. 1992. Cortical local circuit axons do not mature after early deafferentation. Proc Natl Acad Sci USA. 89:1832–1836.
McQuillen PS, Ferriero DM. 2005. Perinatal subplate neuron injury: implications for cortical development and plasticity. Brain Pathol. 15:250–260.
Mégevand P, Quairiaux C, Lascano AM, Kiss JZ, Michel CM. 2008. A mouse model for studying large-scale neuronal networks using EEG mapping techniques. Neuroimage. 42:591–602.
Mégevand P, Troncoso E, Quairiaux C, Muller D, Michel CM, Kiss JZ. 2009. Long-term plasticity in mouse sensorimotor circuits after rhythmic whisker stimulation. J Neurosci. 29:5326–5335.
Michel CM, Murray MM, Lantz G, Gonzalez S, Spinelli L, Grave de PR. 2004. EEG source imaging. Clin Neurophysiol. 115:2195–2222.
Micheva KD, Beaulieu C. 1996. Quantitative aspects of synaptogenesis in the rat barrel field cortex with special reference to GABA circuitry. J Comp Neurol. 373:340–354.
Mitzdorf U. 1985. Current source-density method and application in cat cerebral-cortex—investigation of evoked-potentials and EEG phenomena. Physiol Rev. 65:37–100.
Nudo RJ. 2006. Mechanisms for recovery of motor function following cortical damage. Curr Opin Neurobiol. 16:638–644.
Nudo RJ. 2007. Postinfarct cortical plasticity and behavioral recovery. Stroke. 38:840–845.
Olavarria J, Van Sluyters RC, Killackey HP. 1984. Evidence for the complementary organization of callosal and thalamic connections within rat somatosensory cortex. Brain Res. 291:364–368.
Pihko E, Lauronen L. 2004. Somatosensory processing in healthy newborns. Exp Neurol. 190(Suppl 1):S2–S7.
Rice FL, Van der Loos H. 1977. Development of barrels and barrel field in somatosensory cortex of mouse. J Comp Neurol. 171: 545–560.
Rorke LB. 1992. Anatomical features of the developing brain implicated in pathogenesis of hypoxic-ischemic injury. Brain Pathol. 2:211–221.
Schiene K, Staiger JF, Bruehl C, Witte OW. 1999. Enlargement of cortical vibrissa representation in the surround of an ischemic cortical lesion. J Neurol Sci. 162:6–13.
Schlaggar BL, Fox K, Oleary DDM. 1993. Postsynaptic control of plasticity in developing somatosensory cortex. Nature. 364:623–626.
Schlaggar BL, O'Leary DD. 1994. Early development of the somatotopic map and barrel patterning in rat somatosensory cortex. J Comp Neurol. 346:80–96.
Shuler MG, Krupa DJ, Nicolelis MA. 2001. Bilateral integration of whisker information in the primary somatosensory cortex of rats. J Neurosci. 21:5251–5261.
Simons DJ. 1978. Response properties of vibrissa units in rat Si somatosensory neocortex. J Neurophysiol. 41:798–820.
Sizonenko SV, Camm EJ, Garbow JR, Maier SE, Inder TE, Williams CE, Neil JJ, Huppi PS. 2007. Developmental changes and injury induced disruption of the radial organization of the cortex in the immature rat brain revealed by in vivo diffusion tensor MRI. Cereb Cortex. 18:1444–1454.
Sizonenko SV, Kiss JZ, Inder T, Gluckman PD, Williams CE. 2005. Distinctive neuropathologic alterations in the deep layers of the parietal cortex after moderate ischemic-hypoxic injury in the P3 immature rat brain. Pediatr Res. 57:865–872.
Sizonenko SV, Sirimanne E, Mayall Y, Gluckman PD, Inder T, Williams C. 2003. Selective cortical alteration after hypoxic-ischemic injury in the very immature rat brain. Pediatr Res. 54:263–269.
Stern EA, Maravall M, Svoboda K. 2001. Rapid development and plasticity of layer 2/3 maps in rat barrel cortex in vivo. Neuron. 31: 305–315.
Thairu BK. 1971. Post-natal changes in the somaesthetic evoked potentials in the albino rat. Nat New Biol. 231:30–31.
Towfighi J, Mauger D. 1998. Temporal evolution of neuronal changes in cerebral hypoxia-ischemia in developing rats: a quantitative light microscopic study. Brain Res Dev Brain Res. 109:169–177.
Troncoso E, Muller D, Czellar S, Zoltan KJ. 2000. Epicranial sensory evoked potential recordings for repeated assessment of cortical functions in mice. J Neurosci Methods. 97:51–58.
Troncoso E, Muller D, Korodi K, Steimer T, Welker E, Kiss JZ. 2004. Recovery of evoked potentials, metabolic activity and behavior in a mouse model of somatosensory cortex lesion: role of the neural cell adhesion molecule (NCAM). Cereb Cortex. 14:332–341.
Van der Loos H, Woolsey TA. 1973. Somatosensory cortex: structural alterations following early injury to sense organs. Science. 179: 395–398.
Vanhatalo S, Lauronen L. 2006. Neonatal SEP. Back to bedside with basic science. Semin Fetal Neonatal Med. 11:464–470.
Vannucci RC, Vannucci SJ. 2005. Perinatal hypoxic-ischemic brain damage: evolution of an animal model. Dev Neurosci. 27:81–86.
Volpe JJ. 2009. Brain injury in premature infants: a complex amalgam of destructive and developmental disturbances. Lancet Neurol. 8:110–124.
Welker C. 1971. Microelectrode delineation of fine grain somatotopic organization of Smi cerebral neocortex in albino rat. Brain Res. 26:259–265.
Wise SP, Jones EG. 1978. Developmental studies of thalamocortical and commissural connections in the rat somatic sensory cortex. J Comp Neurol. 178:187–208.
Witte OW, Bidmon HJ, Schiene K, Redecker C, Hagemann G. 2000. Functional differentiation of multiple perilesional zones after focal cerebral ischemia. J Cereb Blood Flow Metab. 20:1149–1165.
Woolsey TA, Van der Loos H. 1970. Structural organization of layer-IV in somatosensory region (S1) of mouse cerebral cortex. Description of a cortical field composed of discrete cytoarchitectonic units. Brain Res. 17:205–242.